Naval Research Laboratory
Washington, DC 20375-5320

NRL/8150/MR—2022/1

Progress Update of Laser-Cooled Rubidium Clock

ROY READY

RUSSELL BRADLEY

SCOTT CRANE (FORMER NRL EMPLOYEE)

Advanced Space Precision Navigation and Timing Branch
Space Systems Development Division

ADAM BLACK

Optical Physics Branch
Optical Sciences Division

February 10, 2022

REPORT DOCUMENTATION PAGE

Form Approved
OMB No. 0704-0188

1. REPORT DATE *(DD-MM-YYYY)*	**2. REPORT TYPE**	**3. DATES COVERED** *(From - To)*
10-02-2022	NRL Memorandum Report	07/06/2021 – 12/13/2021

4. TITLE AND SUBTITLE

Progress Update of Laser-Cooled Rubidium Clock

5a. CONTRACT NUMBER

5b. GRANT NUMBER

5c. PROGRAM ELEMENT NUMBER

6. AUTHOR(S)

Roy Ready, Adam Black, Russell Bradley, and Scott Crane*

5d. PROJECT NUMBER

5e. TASK NUMBER

5f. WORK UNIT NUMBER
1L50

7. PERFORMING ORGANIZATION NAME(S) AND ADDRESS(ES)

Naval Research Laboratory
4555 Overlook Avenue, SW
Washington, DC 20375-5320

8. PERFORMING ORGANIZATION REPORT NUMBER

NRL/8150/MR--2022/1

9. SPONSORING / MONITORING AGENCY NAME(S) AND ADDRESS(ES)

Office of Naval Research
One Liberty Center
875 N. Randolph Street, Suite 1425
Arlington, VA 22203-1995

10. SPONSOR / MONITOR'S ACRONYM(S)

ONR

11. SPONSOR / MONITOR'S REPORT NUMBER(S)

12. DISTRIBUTION / AVAILABILITY STATEMENT

DISTRIBUTION STATEMENT A: Approved for public release; distribution is unlimited.

13. SUPPLEMENTARY NOTES

*Former NRL Employee

14. ABSTRACT

We are developing a cold rubidium clock that will use the quantum entanglement technique of spin squeezing to measure a clock signal to better precision than a conventional (non-entangled) measurement. As a first step, we assembled and validated a laser cooling and trapping scheme to interrogate a cloud of rubidium atoms. In this report, we discuss our work characterizing the initial experimental setup, which is built around a commercial magneto-optical trap that uses magnetic fields and our laser scheme to collect the atoms. Over the course of several months we refined the laser cooling and trapping frequencies, laser powers, associated optics, and electronics. We report an atom loading time as low as 0.5 s and a trap number of several billion rubidium atoms. This is comparable to reported parameters in similar rubidium systems and demonstrates a critical step in developing a cold atom clock. We conclude with an outline of the envisioned next stage of the experiment, where we will demonstrate a baseline clock signal and upgrade the trap apparatus with a custom science chamber.

15. SUBJECT TERMS

16. SECURITY CLASSIFICATION OF:			**17. LIMITATION OF ABSTRACT**	**18. NUMBER OF PAGES**	**19a. NAME OF RESPONSIBLE PERSON**
					Roy Ready
a. REPORT	**b. ABSTRACT**	**c. THIS PAGE**	U	15	**19b. TELEPHONE NUMBER** *(include area code)*
U	U	U			(202) 404-8861

Standard Form 298 (Rev. 8-98)
Prescribed by ANSI Std. Z39.18

This page intentionally left blank.

CONTENTS

This page intentionally left blank

EXECUTIVE SUMMARY

We are developing a cold rubidium clock that will use the quantum entanglement technique of spin squeezing to measure a clock signal to better precision than a conventional (non-entangled) measurement. As a first step, we assembled and validated a laser cooling and trapping scheme to interrogate a cloud of rubidium atoms. In this report, we discuss our work characterizing the initial experimental setup, which is built around a commercial magneto-optical trap that uses magnetic fields and our laser scheme to collect the atoms.

Over the course of several months we refined the laser cooling and trapping frequencies, laser powers, associated optics, and electronics. We report an atom loading time as low as 0.5 s and a trap number of several billion rubidium atoms. This is comparable to reported parameters in similar rubidium systems and demonstrates a critical step in developing a cold atom clock.

We conclude with an outline of the envisioned next stage of the experiment, where we will demonstrate a baseline clock signal and upgrade the trap apparatus with a custom science chamber.

This page intentionally left blank

PROGRESS UPDATE OF LASER-COOLED RUBIDIUM CLOCK

1. INTRODUCTION

Modern atomic clocks include neutral atom ensembles and single ionized atoms operating in the microwave and optical regime. The sensitivity of the clock signals of these systems are ultimately limited by intrinsic noise of the atomic ensemble [1–4]. This intrinsic property of the atoms is known as quantum projection noise (QPN) [5].

In the recently published work of a rubidium fountain atomic clock, the authors load up to 2.4×10^6 atoms with a two-dimensional magneto-optical trap (2D MOT) [2]. The atoms are cooled to 1.6 μK and launched upwards for state preparation using an optical molasses technique. They report a QPN-limited, clock signal fractional frequency instability $\sigma_y \left[\mathrm{s}^{1/2}\right]$ of $3 \times 10^{-14}/\sqrt{\tau_{\mathrm{avg}}}$, where τ_{avg} is the averaging time.

The atom entanglement technique of "spin squeezing" was recently demonstrated for a rubidium clock signal at Stanford [6]. In this proof of principle experiment, the authors used spin squeezing to reduce the clock instability 20 dB below the QPN limit. They report a clock signal fractional instability of $9.7 \times 10^{-11}/\sqrt{\tau_{\mathrm{avg}}}$ using a trapped rubidium cloud of 5×10^5 atoms cooled to 25 μK [6].

The advanced atom clock group (Code 8150) aims to develop a cold rubidium clock that employs spin squeezing to achieve sub-QPN clock instability. We expect to make a clock that is initially comparable to conventional clocks with a carefully designed apparatus. With further refinements of our clock apparatus and and a well-developed spin squeezing protocol, we hope to improve upon the precision achieved by the most sensitive rubidium clocks.

In this report we discuss our recent work in validating the laser scheme and trapping apparatus and optimizing the number of trappable rubidium atoms. We conclude an outline of next steps for improving the apparatus and measuring a clock signal.

2. LASERS AND APPARATUS

We use a two-chamber commercial MOT (Cold Quanta Physics Platform), as shown in fig. 1. Rubidium vapor is generated in the first chamber from a hot dispenser. The atoms are cooled and collimated with counter-propagating lasers and a quadrupolar, 35 Gauss/cm magnetic field forming a 2D MOT. The atom flux is directed through a 0.75 mm aperture connected to the second chamber.

The atoms are captured and further cooled in the second, ultrahigh vacuum chamber, where we form a 3D MOT (fig. 1b). The trapping magnetic field is generated by two rectangular coils on opposing sides of the 3D chamber. The field is approximately 10 Gauss/cm.

We use a 780 nm, 1 W tapered amplifier diode laser (Toptica DL-pro) for atom cooling. Atoms are repumped with a 1560 nm fiber laser that outputs up to 1 W of frequency-doubled light (Quantel EYLSA 780). These lasers are referred to as the "trap laser" and "repump laser," respectively.

Manuscript approved February 1, 2022.

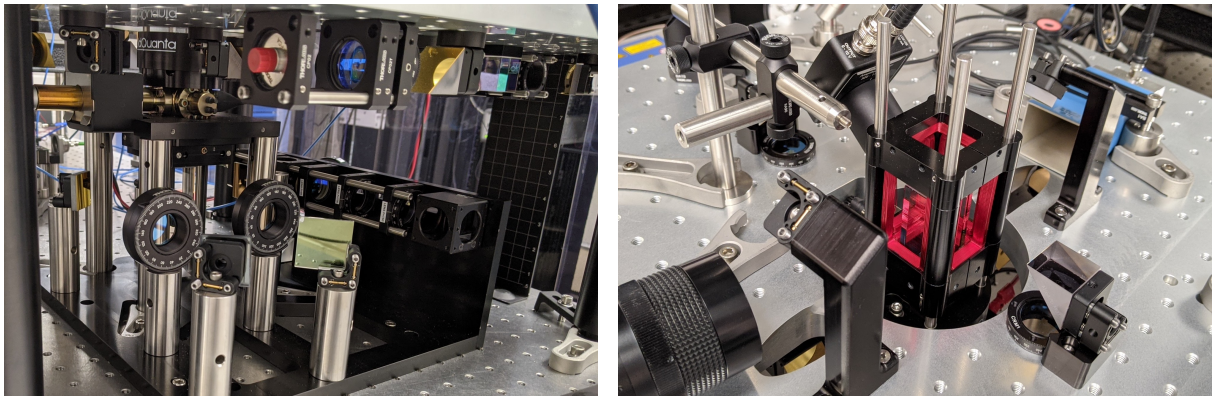

(a) (b)

Fig. 1—Left: the lower 2D MOT loading chamber. Right: the upper 3D MOT trapping chamber. The chambers are connected by a 0.75 mm diameter pinhole.

The trap laser is locked to the ^{87}Rb $^2S_{1/2}$ $(F = 2) \rightarrow {}^2P_{3/2}$ $(F' = 3)$ transition using a Doppler-free reference cell. The repump laser is offset phase locked to the trap laser near the ^{87}Rb $^2S_{1/2}$ $(F = 1) \rightarrow {}^2P_{3/2}$ $(F' = 2)$ transition using commercial beat detection electronics (Vescent D2).

The trap laser is split along two path lengths. About 65% of the laser power is directed along a 2D MOT path and 35% is directed to the 3D MOT path. The laser frequency of each path is independently tuned with an acousto-optic modulator (AOM) in a double-pass configuration. We have a tuning bandwidth of 200 MHz with the double-passed AOMs (G&H AOMO 3080-122).

The repump laser is split along the 2D and 3D MOT paths analogously to the trap laser. The repump light is combined with the frequency-tuned trap laser paths, which are then fiber-coupled to the trapping apparatus. Approximately 25 mW/cm^2 of light is coupled into the 2D MOT and 15 mW/cm^2 is coupled into the 3D MOT.

2.1 Characterization of the magneto-optical trap

We use a gain-switchable photodetector (Thorlabs PDA36A2) with a 1" collection lens to measure the 3D MOT fluorescence. External light is blocked by a lens tube and room lighting is turned off during fluorescence measurements. The photodetector is positioned 150 mm behind the 3D MOT cell as shown in fig. 1b.

To estimate the number of atoms in the trap, we assume that the atom cloud is spherical, that the detector is small and far away compared to the cloud size, and that the atoms in the cloud fluoresce isotropically. Under these conditions, the number of atoms in the trap is given by the following:

$$N = P_{\text{det}} \cdot \frac{1}{\Omega_{\text{det}}} \cdot \frac{1}{h\nu_a} \frac{1}{R} \frac{1}{\epsilon^k}, \tag{1}$$

where

P_{det} [W] is the fluorescent power incident on the photodetector,

Ω_{det} is the solid angle subtended by the photodetector,
$h = 6.626 \times 10^{-34}$ J Hz^{-1} is the Planck constant,
$\nu_a = 384.230 \times 10^{12}$ Hz is the transition frequency of ^{87}Rb(D2),
R $\left[\text{s}^{-1}\right]$ is the steady-state single atom photon scattering rate,
ϵ is the transmission efficiency of light through each transmissive surface between the atoms and the photodetector, and
k is the number of surfaces the light passes through.

The steady-state single atom photon scattering rate is given by the following expression [7]:

$$R = \frac{\Gamma}{2} \frac{(I/I_{\text{sat}})}{1 + 4\,(\Delta/\Gamma)^2 + (I/I_{\text{sat}})}\,, \tag{2}$$

where
$\Gamma = 2\pi \times 6.07$ MHz is the D2 natural linewidth,
I $\left[\text{mW/cm}^2\right]$ is the trap light intensity,
$I_{\text{sat}} = 3.58$ mW/cm^2 is the on-resonance, isotropic saturation intensity of the $(F = 2 \rightarrow F' = 3)$ transition, and
Δ [MHz] is the trap light detuning.

For a trap light intensity of $I = 75\ \text{mW}/(\pi\ 2.5 \times 1.5/4\ \text{cm}^2)$ and a detuning $\Delta = 2.5\Gamma$, eq. (2) gives a photon scattering rate $R \approx 4.1 \times 10^6$ s^{-1}. eq. (1) gives a total atom number $N \approx 10^9$ for a typical photodetector power $P_{\text{det}} \approx 200\ \mu$W.

The total atom rate of the 3D MOT dN/dt $\left[\text{s}^{-1}\right]$ is the balance of the loading rate from the 2D MOT and the loss rate of several processes:

$$\begin{aligned} \frac{dN}{dt} &= \mathcal{R} - \frac{N}{\tau} - \beta \int n^2\,(\vec{r}, t)\, d^3 r\,, \\ \tau &= \frac{\tau_{\text{Rb}}\ \tau_{\text{bg}}}{\tau_{\text{Rb}} + \tau_{\text{bg}}}\,, \end{aligned} \tag{3}$$

where
$\mathcal{R}$ $\left[\text{s}^{-1}\right]$ is the loading rate,
τ_{Rb} [s] is the lifetime limited by rubidium-rubidium collisions,
τ_{bg} [s] is the lifetime limited by rubidium-background gas collisions,
β $\left[\text{cm}^3\ \text{s}^{-1}\right]$ is the light-assisted collisional loss coefficient, and
$n\,(\vec{r}, t)$ $\left[\text{cm}^{-3}\right]$ is the density number at position $\vec{r}$.

MOT loading times need to be short enough to saturate the trap before longer timescale effects limit the atom number. Rubidium loading times have been reported in the range of 0.2–3 s [8–10].

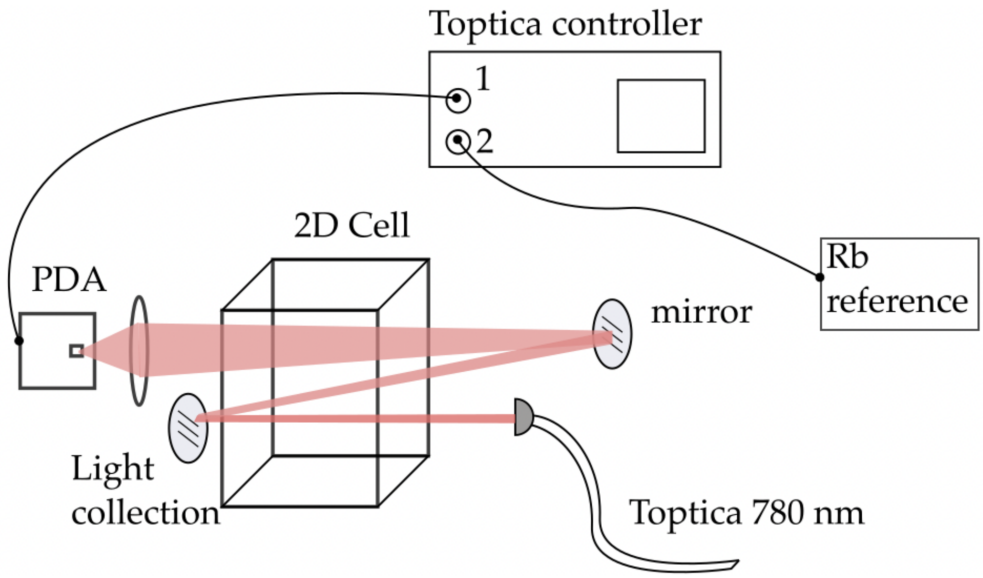

Fig. 2—Schematic of the saturation spectroscopy setup. 10 μW of the trap laser is coupled to the 2D vapor cell. The beam slowly diverges as it passes through the vapor cell multiple times. The trap laser ("Toptica") controller continuously scans while recording the absorption signal of both the 2D cell and Doppler-free Rb reference.

2.2 Rubidium vapor pressure

The trap loading rate depends on the atomic flux through the pinhole connecting the two MOT chambers. The flux depends on the rubidium vapor pressure in the 2D chamber. We assembled a Doppler-limited saturation spectroscopy setup to measure the vapor pressure of the 2D MOT cell. From discussions with colleagues with similar setups, we consider absorption "hole" depths of 15–20% to be a good indicator that the vapor pressure is sufficiently high for our purposes.

A schematic of the setup is shown in fig. 2. We couple approximately 10 μW of trap light through the cell and continuously scan the laser over the ^{85}Rb and ^{87}Rb D2 transitions. The beam intensity is initially $\leq 1.7\text{mW/cm}^2$, though there is visible divergence after the second path length through the cell. Rubidium vapor is generated by supplying 0–3.5 A through the dispenser heating element. The absorption line(s) are detected by an amplified photodiode (Thorlabs PDA36A2).

First, we performed a "narrow" scan, which captures the $^{87}\text{Rb}\ ^2\text{S}_{1/2}\ (F = 2) \rightarrow\ ^2\text{P}_{3/2}$ transition. This scan does not require modification of the diode laser settings. A plot of the absorption signal for different vapor cell currents is shown in fig. 3. The Doppler-broadened peak width is approximately 400 MHz and completely obscures hyperfine spectra.

The reference cell gives a Doppler-free, hyperfine-resolved fluorescence spectrum and sets the laser piezo-frequency scale. Using the hyperfine peaks as reference points, we performed a linear fit to find a scale of 418 ± 7 MHz/V. With zero vapor cell current, the laser intensity is relatively flat over the laser scan range.

At currents greater than 2.5 A, a broad absorption hole can be seen. At a current of 3.5 A, the relative depth of the hole is approximately 35% of the laser intensity. This is consistent with our colleagues' observations of their similar MOT apparatus.

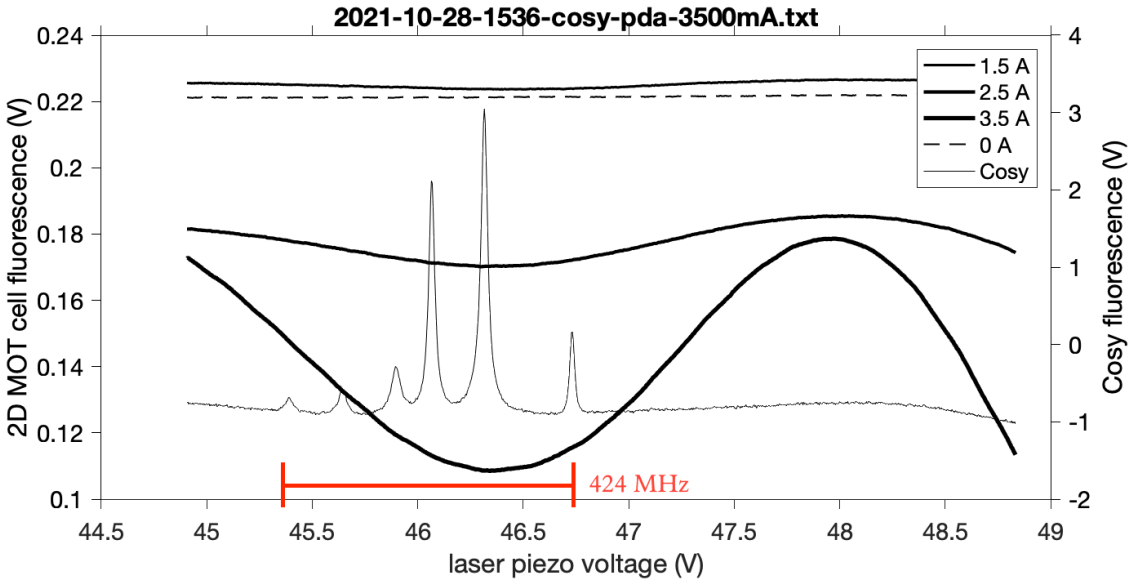

Fig. 3—Absorption profile of the ^{87}Rb $^{2}S_{1/2}$ $(F = 2) \rightarrow {}^{2}P_{3/2}$ transition. Left axis: several Doppler-limited saturation spectroscopy measurements at different oven currents. Right axis: Doppler-free reference spectrum (Cosy), which reveals the hyperfine splittings.

We repeated the absorption measurement with a full scan (6.5 GHz) over all D2 transitions. To suppress mode-hops over the relevant scan range, we scaled the chip current with the laser piezo scanning voltage by a "feed-foward" factor.

The full-scan absorption profiles are shown in fig. 4. The manufacturer-recommended operating range is 3.2–3.7 A. We measured the absorption at zero current, 100 mA, 700 mA, 1300 mA, then varied the vapor cell current in 300 mA steps to a maximum of 3.7 A.

Our measurements yield absorption lines at vapor cell currents as small as 1.3 A, though the true minimum current may be smaller. At a cell current of 2.8 A, the ^{87}Rb $^{2}S_{1/2}$ $(F = 2)$ relative hole depth is $\approx 8\%$. At 3.1 A, the depth is $\approx 14\%$.

Following the absorption spectroscopy measurements, we measured the 3D MOT fluorescence with a vapor cell current at 2.8 A and then at 3.1 A. Curiously, the measured fluorescence did not increase significantly when increasing the current. This may suggest that the atomic flux through the chamber pinhole is saturated, or perhaps the 3D MOT trapping efficiency can be further optimized.

3. DATA AND ANALYSIS

3.1 Measuring the trap load time and lifetime

We define the MOT load time $\tau^{\star}$ as the characteristic time it takes to load the trap to $1/e$ of the maximum atom number. We define the lifetime τ as the characteristic time it takes for the maximum atom number to decay by $1/e$ after switching off the 2D trap light.

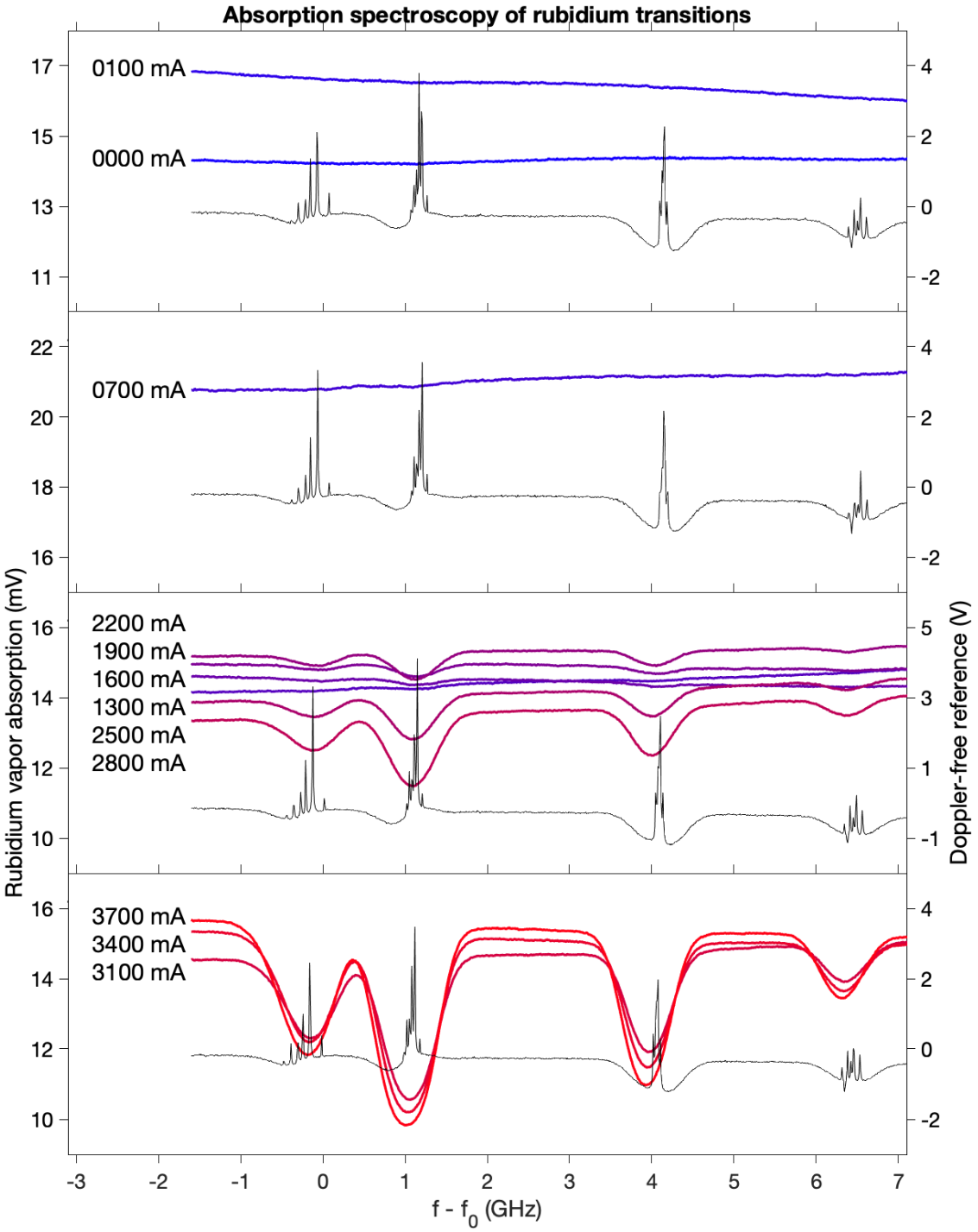

Fig. 4—Wide scan of the rubidium absorption profile for a range of rubidium cell currents, up to the manufacturer-specified limit of 3.7 A. The horizontal scale is the fitted laser frequency relative to the clock transition $^{87}\mathrm{Rb}\ ^2\mathrm{S}_{1/2}\ (F = 2) \rightarrow {}^2\mathrm{P}_{3/2}\ (F' = 3)$. From left to right, the Doppler-limited transitions are: $^{87}\mathrm{Rb}\ ^2\mathrm{S}_{1/2}\ (F = 2) \rightarrow {}^2\mathrm{P}_{3/2}$, $^{85}\mathrm{Rb}\ ^2\mathrm{S}_{1/2}\ (F = 3) \rightarrow {}^2\mathrm{P}_{3/2}$, $^{85}\mathrm{Rb}\ ^2\mathrm{S}_{1/2}\ (F = 2) \rightarrow {}^2\mathrm{P}_{3/2}$, $^{87}\mathrm{Rb}\ ^2\mathrm{S}_{1/2}\ (F = 1) \rightarrow {}^2\mathrm{P}_{3/2}$.

The load time and lifetime is averaged over a series of consecutive atom trap loading and extinguishing intervals. The 3D trap laser is held to its optimized trapping frequency throughout the measurements. The loading sequence is initiated by ramping the 2D trap laser to the optimized trapping frequency. The 3D MOT atom signal is measured by a photodetector as shown in fig. 1b. Once the trap is saturated, the 2D trap laser AOM tuning voltage is set to zero, or 'switched off,' to attenuate atom loading. The lifetime sequence is the following time interval during which the 3D MOT atom signal decays.

We fit the photodetector signal (proportional to the number of atoms) with exponential fitting functions to find the characteristic loading time $\tau^\star$ [s] and lifetime τ [s] of a measurement, consistent with literature [9]:

$$\begin{aligned} N_{\text{load}}(t) &= \left[C + A \cdot \left(1 - \exp\left\{-\frac{t}{\tau^\star}\right\}\right)\right] \cdot (1 + B \sin(\omega t + \phi)) \ , \\ N_{\text{life}}(t) &= \left(C + A \exp\left\{-\frac{t}{\tau}\right\}\right) \cdot (1 + B \sin(\omega t + \theta)) \end{aligned} \tag{4}$$

The extra sinusoidal factor accounts for a "mystery signal" with frequency $\omega \approx 2\pi \times 0.1$ Hz that is present in our atom trap signal. This signal scales with the fluorescence signal and appears in both the loading and lifetime sequences. We are continuing to investigate the mystery signal in parallel with our other efforts.

A load time sequence depicting our fit to the measured trap atom number vs. time after switching on the trap laser is shown in fig. 5a. In general, the load rate $\mathcal{R}$ depends on the 2D MOT pressure, geometry, rubidium vapor temperature, and the number of atoms in the 3D trap. At times $t < \tau^\star$, the load rate is approximately linear. The initial loading rate $\mathcal{R}_i = A/\tau^\star$ is shown as a dashed linear green slope. As seen in the residual subplot, the fitting function from eq. (4) matches the loading data to within 10%.

A corresponding lifetime measurement is shown in fig. 5b. There is noticeable slippage in the fit to the mystery signal, suggesting some correlation between the mystery signal and the presence of the 2D trap laser.

3.2 Improving the trap load time

We refined the associated optics, fluorescence imaging, and lasers over a period of several months to improve our loading time $\tau^\star$. We took benchmark load time tests on an approximately weekly basis to track the performance as changes were implemented. Some of these changes include: adjusting the photodetector position and angle, adjusting the light collection lens position and focal length choice, tuning the AOM frequency, tuning the trap and repump laser power settings, optimizing the MOT magnetic field coil current, and tuning the offset locking RF frequency.

A track record of the load time as changes are implemented is shown in fig. 6. The adjustments to the apparatus result in a steady reduction in loading time. Our initial loading time was $\approx$ 16 s, but we now routinely observe load times of 0.5–1 s.

The evolution of the atom trap shape is shown in fig. 7. The atom cloud is quite diffuse in our baseline rough alignment, indicating a low atom number. We temporarily lost the MOT signal while refining the trap laser stability. While the initial recovered trap is noticeably smaller than the baseline trap, it is brighter (denser) in the center. The atom cloud becomes larger, approximately 1 cm in diameter, and more symmetric as the trapping optics are calibrated.

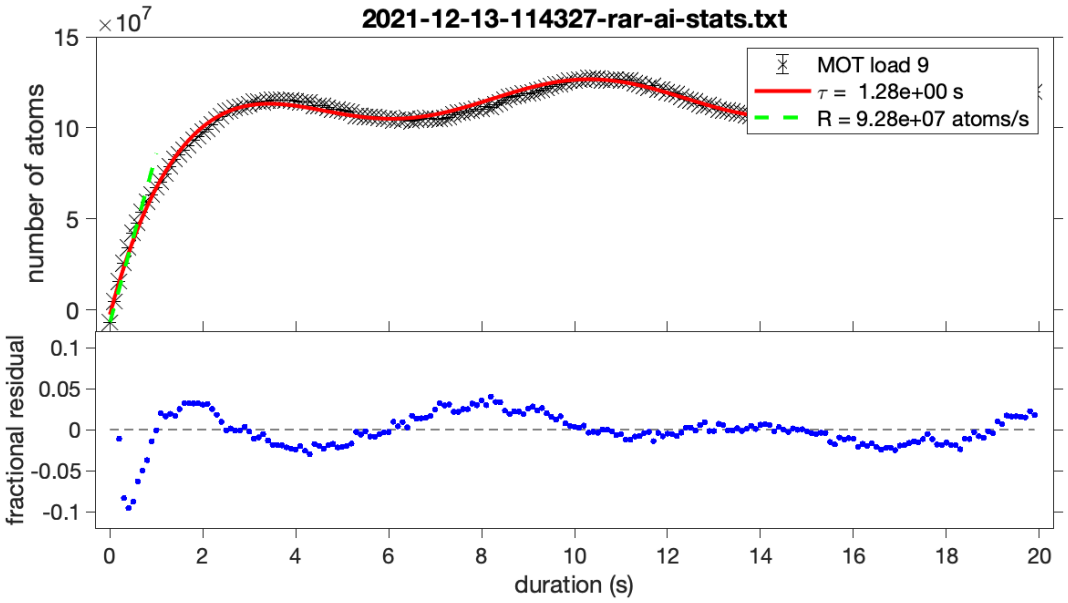

(a)

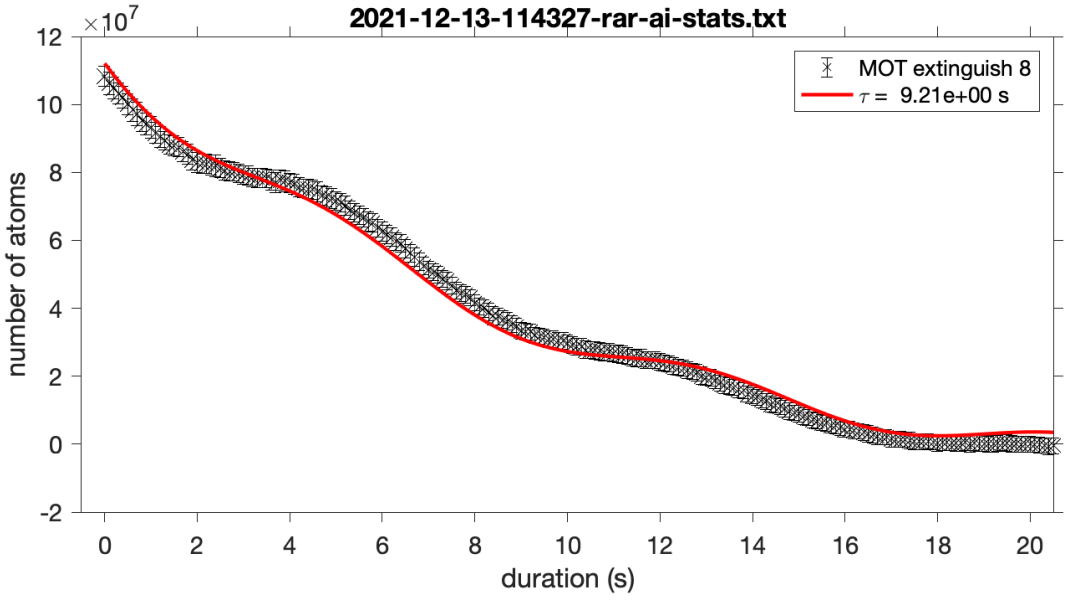

(b)

Fig. 5—(a) A fit to a selected 3D MOT loading sequence. The bottom half of the plot is the relative deviation of the fit from the data. (b) A fit to a selected 3D MOT lifetime sequence.

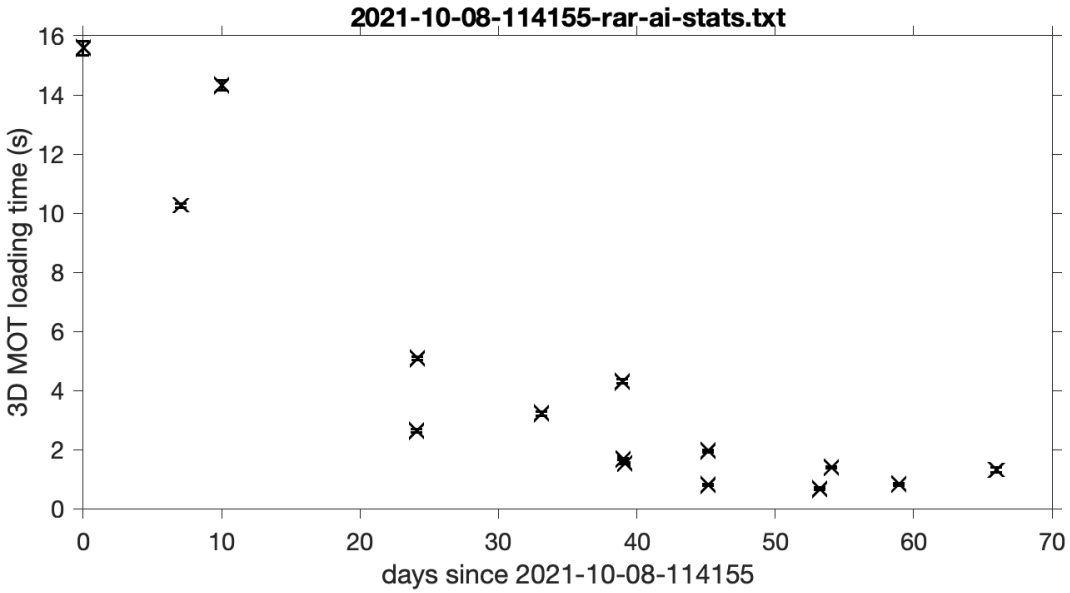

Fig. 6—The rubidium MOT load time as improvements to the apparatus are made over the course of several months. The trapping laser powers and repump laser power are tuned each week. Other small optimizations of the apparatus are made throughout this time. Notable changes are listed in what follows. Day 24: refined 2D MOT beam alignment, refined 2D stage positioning. Day 33: refined 3D MOT beam alignment, refined magnetic field supply current, refined pump laser frequency. Day 45: implement 2D MOT push beam.

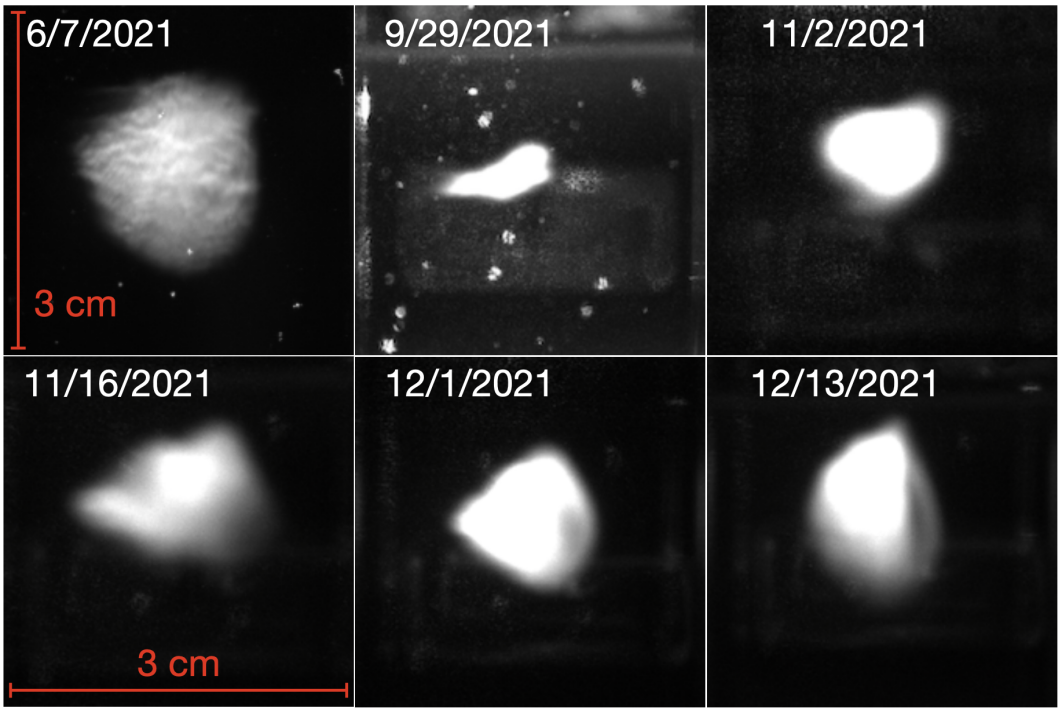

Fig. 7—Snapshots of the rubidium cloud confined in a 3D MOT as the lasers and optics are refined over a six-month period.

The initial load rates $\mathcal{R}_i$, lifetimes, and upper limit atom trap numbers $N_{\max} = \mathcal{R}_i \tau$ of a handful of systems are shown in table 1. Our best load rate and maximum atom number is comparable to other reports in similar systems and is consistent with the manufacturer specifications.

We note that the global maximum load rate of 8.4×10^{10} atoms/s [9] and global maximum lifetime of 240 s [8] are more than an order of magnitude larger than our parameters. This suggests that additional significant improvements can be made to our system.

Table 1—A non-exhaustive list of magneto-optical trap parameters of similar rubidium systems.

$\mathcal{R}_i$ $(\times 10^7$ atoms/s)	lifetime (s)	$N_{\max}$ $(\times 10^7)$	Reference
8400	2	800	[9]
	240	500	[8]
1	9	10	[11]
> 10	100	> 50	manufacturer data sheet
20	15	300	This work

4. CONCLUSIONS AND NEXT STEPS

We successfully demonstrated a laser locking scheme for cooling and trapping rubidium in a commercial, double chamber magneto-optical trap. Over the course of several months, we refined the optical characteristics of the apparatus to improve atom loading times by more than a factor of 16. We can currently trap up to an estimated several billion atoms within several seconds, consistent with reports of similar systems.

We are targeting several objectives along the path to a high precision cold rubidium clock measurement. First, we will assemble and validate a new high-finesse optical cavity that will stabilize the lasers and serve as the science chamber for cooling and trapping rubidium. The custom cavity design is completed and the parts have already been machined. At the same time, we will measure the temperature of our commercial trap using a compressed magneto-optical trap technique. Then, we will demonstrate a conventional Ramsey interference clock signal.

Further down the line, we will assemble a science chamber with the custom optical cavity. We will reproduce and improve our clock signal with the new apparatus. Once we've demonstrated a clock signal in the new science chamber, we will be well-positioned to implement spin squeezing to reduce the clock instability below the quantum projection noise limit.

5. ACKNOWLEDGEMENTS

We'd like to thank Jonathan Kwolek (code 5610) and Sunil Upadhyay (code 5610) for lending their expertise to our optical circuit design and diagnosis of our MOT performance.

This work is funded by New Start 6.1 Base Program: Advanced Clocks Based on Quantum Entangled Atoms.

REFERENCES

1. V. Gerginov, N. Nemitz, S. Weyers, R. Schröder, D. Griebsch, and R. Wynands, "Uncertainty evaluation of the caesium fountain clock PTB-CSF2," *Metrologia* **47**(1), 65–79 (dec 2009), doi:10.1088/0026-1394/47/1/008. URL https://doi.org/10.1088/0026-1394/47/1/008.

2. J. Guéna, M. Abgrall, A. Clairon, and S. Bize, "Contributing to TAI with a secondary representation of the SI second," *Metrologia* **51**(1), 108–120 (jan 2014), doi:10.1088/0026-1394/51/1/108. URL https://doi.org/10.1088/0026-1394/51/1/108.

3. S. M. Brewer, J. S. Chen, A. M. Hankin, E. R. Clements, C. W. Chou, D. J. Wineland, D. B. Hume, and D. R. Leibrandt, "$^{27}Al^{+}$ Quantum-Logic Clock with a Systematic Uncertainty below 10^{-18}," *Phys. Rev. Lett.* **123**, 033201 (Jul 2019), doi:10.1103/PhysRevLett.123.033201. URL https://link.aps.org/doi/10.1103/PhysRevLett.123.033201.

4. E. Oelker, R. Hutson, C. Kennedy, L. Sonderhouse, T. Bothwell, A. Goban, D. Kedar, C. Sanner, J. Robinson, G. Marti, et al., "Demonstration of 4.8× 10- 17 stability at 1 s for two independent optical clocks," *Nature Photonics* **13**(10), 714–719 (2019).

5. W. M. Itano, J. C. Bergquist, J. J. Bollinger, J. M. Gilligan, D. J. Heinzen, F. L. Moore, M. G. Raizen, and D. J. Wineland, "Quantum projection noise: Population fluctuations in two-level systems," *Phys. Rev. A* **47**, 3554–3570 (May 1993), doi:10.1103/PhysRevA.47.3554. URL https://link.aps.org/doi/10.1103/PhysRevA.47.3554.

6. O. Hosten, N. J. Engelsen, R. Krishnakumar, and M. A. Kasevich, "Measurement noise 100 times lower than the quantum-projection limit using entangled atoms," *Nature* **529**(7587), 505–508 (2016). URL https://doi.org/10.1038/nature16176.

7. D. A. Steck, "Rubidium 87 D line data, revision 2.2.1, 21 November 2019," 2001. URL http://steck.us/alkalidata.

8. M. H. Anderson, W. Petrich, J. R. Ensher, and E. A. Cornell, "Reduction of light-assisted collisional loss rate from a low-pressure vapor-cell trap," *Phys. Rev. A* **50**, R3597–R3600 (Nov 1994), doi:10.1103/PhysRevA.50.R3597. URL https://link.aps.org/doi/10.1103/PhysRevA.50.R3597.

9. S. Jöllenbeck, J. Mahnke, R. Randoll, W. Ertmer, J. Arlt, and C. Klempt, "Hexapole-compensated magneto-optical trap on a mesoscopic atom chip," *Phys. Rev. A* **83**, 043406 (Apr 2011), doi:10.1103/PhysRevA.83.043406. URL https://link.aps.org/doi/10.1103/PhysRevA.83.043406.

10. E. A. Salim, *Ultracold matter systems and atomtronics instrumentation.*, PhD thesis (University of Colorado at Boulder, 2011).

11. J. R. Ensher, *The first experiments with Bose-Einstein condensation of rubidium-87*, PhD thesis (UNIVERSITY OF COLORADO AT BOULDER, Oct. 1999).